

A lower mass for the exoplanet WASP-21b

S. C. C. Barros^{1*}, D. L. Pollacco¹, N. P. Gibson^{1,2}, I. D. Howarth³, F. P. Keenan¹,
E. K. Simpson¹, I. Skillen⁴, I. A. Steele⁵

¹*Astrophysics Research Centre, School of Mathematics and Physics, Queen's University Belfast, University Road, Belfast, BT7 1NN, UK*

²*Department of Physics, University of Oxford, Denys Wilkinson Building, Keble Road, Oxford OX1 3RH, UK*

³*Department Physics and Astronomy, UCL, Gower Street, London WC1E 6BT, UK*

⁴*Isaac Newton Group of Telescopes, Apartado de Correos 321, E-38700 Santa Cruz de la Palma, Tenerife, Spain*

⁵*Astrophysics Research Institute, Liverpool John Moores University, CH61 4UA, UK*

Accepted . Received ; in original form

ABSTRACT

We present high precision transit observations of the exoplanet WASP-21b, obtained with the RISE instrument mounted on 2.0m Liverpool Telescope. A transit model is fitted, coupled with an MCMC routine to derive accurate system parameters. The two new high precision transits allow to estimate the stellar density directly from the light curve. Our analysis suggests that WASP-21 is evolving off the main sequence which led to a previous overestimation of the stellar density. Using isochrone interpolation, we find a stellar mass of $0.86 \pm 0.04 M_{\odot}$ which is significantly lower than previously reported ($1.01 \pm 0.03 M_{\odot}$). Consequently, we find a lower planetary mass of $0.27 \pm 0.01 M_{\text{Jup}}$. A lower inclination (87.4 ± 0.3 degrees) is also found for the system than previously reported, resulting in a slightly larger stellar ($R_* = 1.10 \pm 0.03 R_{\odot}$) and planetary radius ($R_p = 1.14 \pm 0.04 R_{\text{Jup}}$). The planet radius suggests a hydrogen/helium composition with no core which strengthens the correlation between planetary density and host star metallicity. A new ephemeris is determined for the system, i.e., $\hat{O} = 2455084.51974 \pm 0.00020$ (HJD) and $P = 4.3225060 \pm 0.0000031$ days. We found no transit timing variations in WASP-21b.

Key words: stars: planetary systems – stars: individual (WASP-21) – techniques: photometric

1 INTRODUCTION

Transiting planet systems are valuable because their geometry enables us to estimate accurate planetary properties. Time-series photometry during the transit allows us to derive the orbital inclination and the relative radii of the host star and planet. Combining this with radial velocity variations and stellar parameters, allows us to derive the absolute mass of the planet. Hence, the bulk density of the planet can be estimated with good accuracy, giving us insight into its composition (Guillot 2005; Fortney et al. 2007), thus placing constraints on planetary structure and formation models. Given the remarkable diversity in the structure of large planets, it is important to obtain planetary parameters which are as accurate as possible. However, obtaining high signal-to-noise transit observations is difficult and consequently even some of the brightest stars with planets are lacking good quality light curves and, hence, have poorly determined planetary parameters.

The RISE (Rapid Imager to Search for Exoplanets) instrument, mounted on the 2.0m Liverpool telescope (Steele et al. 2008; Gibson et al. 2008) was designed for exoplanet transit observations. Its main scientific driver was the detection of transit-timing

variations and hence the search for low-mass companions to “hot Jupiters”. RISE has a rapid readout frame transfer CCD and in 2×2 binned mode has a readout time of less than 1 s. This implies that for exposures longer than 1 s, dead time is negligible substantially increasing the time on target. However, most exoplanet host stars are relatively bright and saturate the CCD for 1 second exposure. To avoid dead time losses, RISE observations are always defocused (e.g. Gibson et al. 2008; Joshi et al. 2009). Defocused photometry observations have also the advantage of spreading the PSF over a larger number of pixels, thereby decreasing flat-fielding errors. RISE is therefore ideal for obtaining high quality transit light curves for exoplanets.

WASP-21b is a Saturn-mass planet with $M_p = 0.30 \pm 0.01 M_{\text{Jup}}$ in a 4.3 day circular orbit (Bouchy et al. 2010). Its host star is a G3V type with $M_* = 1.01 \pm 0.03 M_{\odot}$, $T_{\text{eff}} = 5800 \pm 100$ K and a low metallicity, $[M/H] = -0.4 \pm 0.1$. It was discovered by the SuperWASP-North survey (Pollacco et al. 2006) in its 2008-2009 observing campaign. Bouchy et al. (2010) argue that WASP-21 is a member of the galactic thick disc because of its low metal abundances, velocity relative to the Sun and age ~ 12 Gyr, which are similar to the thick disc population. WASP-21b is among the lowest density planets, $\rho_p = 0.24 \pm 0.05 \rho_J$ (Bouchy et al. 2010), and has one of the lowest metallicity host stars. Therefore, its prop-

* E-mail: s.barros@qub.ac.uk

erties are particularly important for irradiation models. The current parameters of the system (Bouchy et al. 2010) are based on the SuperWASP discovery photometry and a partial transit light curve taken with RISE. However, the lack of a high precision complete transit light curve required the assumption of the main sequence mass-radius relation which tends to bias the estimate of the inclination. Furthermore, the age derived for WASP-21 is longer than the main-sequence life time of a $1.01M_{\odot}$ star. This suggests that WASP-21 could be evolved which would invalidate the main-sequence assumption and bias the parameters of the system. To test the main-sequence assumption we obtained further observations of WASP-21.

In this paper, we present transit observations of WASP-21b with RISE including a full transit light curve. Our high precision light curves allow us derive the planetary and stellar radii without assuming the main-sequence mass-radius relation for the host star. We describe our observations in Section 2. In Section 3, we discuss our transit model and present the updated parameters of the system in Section 4. Finally, we discuss and summarise our results in Section 5.

2 OBSERVATIONS

WASP-21b was observed with RISE (Steele et al. 2008) mounted at the auxiliary Cassegrain focus of the robotic 2.0m Liverpool Telescope on La Palma, Canary Islands. This is a focal reducer system utilizing a frame transfer e2v CCD sensor. The detector has a pixel scale of 0.54 arcsec/pixel that results in a 9.4×9.4 arcmin field of view. RISE has a wideband filter covering $\sim 500\text{--}700$ nm which corresponds approximately to V+R. The instrument has no moving parts.

The Liverpool Telescope has a library of flat fields which are taken manually every couple of months. RISE flats are taken during twilight at different rotator angles so that there is a uniform illumination of the CCD. The exposure times of the images are automatically adjusted so that the peak counts in the individual flats are below the non-linearity limit of the CCD at 45000 counts. Typically, the individual flats have between 20000 and 40000 counts. Due to the fast readout, we can obtain approximately 200 flat frames in a run, these are combined to create a master flat. For each observation run we use the master flat that is closest in time, although we note that these are very stable.

On 2009-09-09 we obtained a full transit of WASP-21b. A total of 6581 exposures in the 2×2 binning mode with an exposure time of 2.7 seconds were taken. The telescope was defocused by -1.2mm which resulted in a FWHM of $\sim 11''$. For defocused photometry, the star profiles are not Gaussian. However, we found that, in our case, a Gaussian provided a good fit to the wings of the star profile, and could be used as a rough estimate of the profile width. Therefore, we estimated the FWHM in the usual way by cross-correlating a Gaussian profile with that of the star.

A second full transit observation of WASP-21b was attempted on 2010-11-24. In this case, deteriorating weather terminated the observations shortly after the mid-transit, by which time, 4008 integrations had been obtained. During these observations, the FWHM was $\sim 12.5''$.

Both data-sets were reduced using the ULTRACAM pipeline (Dhillon et al. 2007) which is optimized for time-series photometry. Initially, we bias subtracted the data while we investigated systematic effects that were introduced by the flat fielding process. We performed differential photometry relative to five comparison

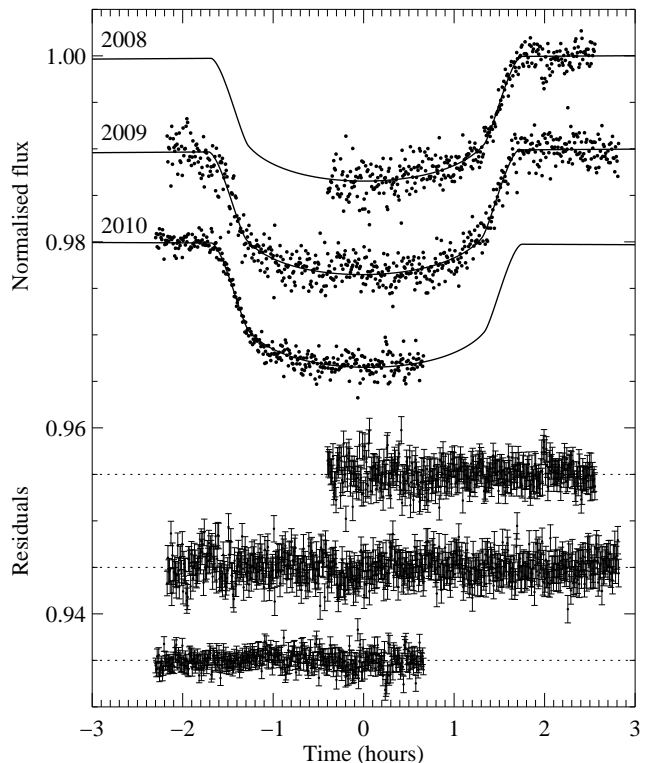


Figure 1. Phase-folded RISE light curves for WASP-21. From top to bottom in chronological order; 2008 October 07, 2009 September 09 and 2010 November 24. We superimpose the best-fit transit model and also show the residuals for each light curve at the bottom of the figure. The data are binned into 30 second periods, and bins displaced vertically for clarity. The individual RISE light curves plotted here are available in electronic form at CDS.

stars in the field, confirmed to be non variable, and we sampled different aperture radii and chose the aperture radius that minimised the noise. For the first night, we used a 22 pixel aperture radius ($\sim 12''$), and for the second transit, a 32 pixel aperture radius ($\sim 17''$). The photometric errors include the shot noise, readout and background noises.

We also included in our analysis, the previously published egress of WASP-21 taken with RISE (Bouchy et al. 2010). For consistency, we re-reduced the original data using the same method as for the other two observations. On 2008-10-07, 2220 exposures of 5 sec duration were taken. We estimated a FWHM of $\sim 2.7''$, therefore, the level of defocussing was lower than in our observations. The best aperture radius was found to be 15 pixel ($\sim 8''$). Our results agree well with the previous published light curve.

The final high precision photometric light curves are shown in Figure 1 along with the best-fit model described in Section 3.3. We overplot the model residuals and the estimated uncertainties which are discussed in Section 3.2.

2.1 Optimum exposure time for RISE

As mentioned above, defocusing is commonly used in exoplanet transit observations. Southworth et al. (2009) calculated the optimum exposure time for the DFOSC imager mounted on the 1.54m Danish Telescope. We follow the same procedure and apply it to RISE mounted on the Liverpool Telescope and hence, we account for readout noise, photon, background and scintillation noise. Sim-

ilar to Southworth et al. (2009), we do not include flat-fielding noise, assuming that the profile position is stable.

The key difference is that RISE is a frame transfer CCD whose dead time is the frame transfer time, 35 milliseconds for observations longer than 1 second. For the brightest comparison star in our field, ($V \approx 9$), we found the optimum exposure times with RISE are approximately 2.7, 7.8, 10.8 seconds during bright, gray and dark time, respectively.

We iterate that the improvement in signal-to-noise for defocused observations, reported by Southworth et al. (2009) is only due to deadtime losses; hence, the defocussing needed is proportional to the CCD readout time. If the deadtime was zero the best theoretical signal-to-noise would always be for focused observations, mainly due to the increase in background noise for wider profiles.

Moreover, in our case, the improvement on signal-to-noise between 1 second and 10.8 seconds exposure times is quite small on the order of 10 ppm per 30 sec bin. As we will see below, the strongest reason for defocussing is to minimise systematic noise which, due to its nature, is not accounted for in the calculation and can substantially increase the noise in a transit light curve. Figure 2 shows systematic noise variations larger than 400 ppm.

3 DATA ANALYSIS

3.1 Systematic noise

Exoplanet transit observations are often dominated by systematic noise. Therefore, to improve the precision of the light curves it is important to determine and minimise this noise source. For the 2009 September 09 observations, the brightest comparison star (c1) on the field was affected by systematic noise. This can clearly be seen in Figure 2, where we show the flux of c1 relative to the ensemble of comparison stars used in the final 2009 WASP-21 light curve. This shows a variation of 400 ppm. We found that this systematic noise was correlated with the star position in the CCD, which during the transit observation varied by 10 pixels in the x direction and 8 in the y . Given that we used an aperture radius of 22 pixels, this implies that only half of the pixels used to perform aperture photometry were common for the duration of the observation. Hence, we concluded that the systematic noise was due to variations in the pixel-to-pixel sensitivity which were not corrected by flat fielding. In fact, the systematic noise is slightly higher if we flat field the data. Our master flat is a combination of 150 frames, each with a mean of 35000 counts. The uncertainty in this flat is 0.5 millimag per pixel which is smaller than the photometric error (~ 4.4 millimag per unbinned point) and the observed systematic noise. After careful analysis of the data, we found that the c1 comparison star crossed a reflection feature in the CCD that is rotator dependent (LT is on an alt-azimuth mount) and thus was not corrected by flat fielding. This experience demonstrates the importance of good guiding in decreasing the sources of systematic noise. If the observations were performed in focus and assuming the seeing was 1 arcsec, the FWHM would have been ~ 2 pixels. Using an aperture radius of $1.5 \times \text{FWHM} = 3$ pixels, it would have implied that there were no common pixels during the observations. Therefore, we infer, if the observations were focused, the amount of systematic noise would have doubled. Note that the defocussing does not affect the guiding since the guide camera is always kept in focus.

After this incident the RISE instrument was upgraded. The source of the reflected feature was identified and removed from the

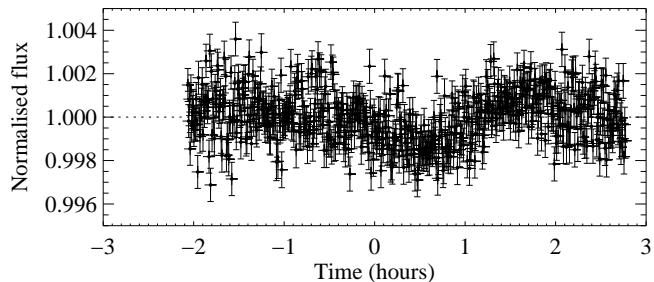


Figure 2. Light curve of the brightest comparison star for the 2009 September 09 observation relative to the ensemble of comparison stars used in WASP21b final light curve. It shows systematic noise with an amplitude of 400 ppm. This comparison was not used in the final light curve of WASP-21. We also overplot the photometric errors.

instrument field of view. We also improved the telescope guiding system’s stability. This led to an improvement in the precision of the light curves which is evident in the latest light curve of WASP-21 taken after the upgrades (see Fig. 1). In the November 2010 observations the variation in position is less than 2 pixels in the x direction and 4 pixels in the y .

3.2 Photometric errors

An accurate estimate of the photometric errors is important to obtain reliable system parameters. Our first estimate of errors for each light curve includes only the shot noise, readout and background noise, which underestimates the true errors. To obtain a more reliable estimate we begin by scaling the errors of each light curve so that the reduced χ^2 of the best fitting model is 1.0. This resulted in the multiplication of the errors by 1.97, 1.22 and 1.44, for the 2008, 2009 and 2010 light curves, respectively. We then calculated the time-correlated noise following the procedure from Gillon et al. (2009). Using the residuals of the best fit model, we estimated the amplitude of the red noise, σ_r to be 150 ppm, 250 ppm and 150 ppm, for the 2008, 2009 and 2010 light curves, respectively. These were added in quadrature to the rescaled photometric errors and were used in the final Markov Chain Monte Carlo (MCMC) chains. However, Carter & Winn (2009) found that this “time-averaging” method of estimating the correlated noise can still underestimate the uncertainties by 15-30 per cent.

3.3 Determination of system parameters

To determine the planetary and orbital parameters, we fitted the three RISE light curves of WASP-21b simultaneously. We used the Mandel & Agol (2002) transit model parametrised by the normalised separation of the planet, a/R_* , ratio of planet radius to star radius, R_p/R_* , orbital inclination, i , and the transit epoch, T_0 , of each light curve. Our model was originally developed to measure transit timing variations of exoplanets. Following Bouchy et al. (2010) that found no evidence for a significant orbital eccentricity of WASP-21b we adopt a circular orbit. We included the quadratic limb darkening (LD) coefficients for the RISE filter V+R from the models of Howarth (2011): $a = 0.45451$ and $b = 0.210172$. These were calculated for $T_{eff} = 5800$ K, $\log g = 4.2$ and $[M/H] = -0.5$ to match the stellar parameters from Bouchy et al. (2010). We initially kept the limb darkening parameters fixed during the fit. For each light curve, we included two extra parameters to account for a linear normalization. Therefore, 12 parameters were fitted. Besides

the linear normalization, no extra trends were removed from the light curve.

To obtain the best fit parameters and uncertainties, we used a MCMC algorithm (e.g. Tegmark et al. 2004; Collier Cameron et al. 2007; Gibson et al. 2008). We begin by calculating the χ^2 statistic of a set of proposed parameters,

$$\chi^2 = \sum_{j=1}^N \frac{(f_j - m_j)^2}{\sigma_j^2}, \quad (1)$$

where f_j is the flux observed at time j , m_j is the model flux and σ_j is the uncertainty of each f_j as described in Section 3.2. At each step in the MCMC chain, each proposed parameter is perturbed by a random amount which we call a “jump function”. Each jump function is proportional to the uncertainty of each parameter multiplied by a random Gaussian number with mean zero and unit standard deviation. The new parameter set is accepted with probability,

$$P = \min \left(1, \exp \left(\frac{-\Delta\chi^2}{2} \right) \right), \quad (2)$$

where $\Delta\chi^2$ is the difference in the χ^2 of subsequent parameters sets. Note, the new parameter set is always accepted if its χ^2 is lower than the previous parameter set ($P = 1$). The jump functions are scaled by a common factor in order to ensure that 25% of the steps are accepted, as suggested by Tegmark et al. (2004). To estimate the uncertainty of each parameter and calculate the jump functions, an initial MCMC fit was performed. With these jump functions, we computed seven MCMC chains each of 150 000 points and different initial parameters. The initial 20% of each chain that corresponded to the burn in phase were discarded and the remaining parts merged into a master chain. We estimated the best fit parameter as the mode of its probability distribution and the 1σ limits as the value at which the integral of the distribution equals 0.341% from both sides of the mode. We computed the Gelman & Rubin (1992) statistic for each fitted parameter and concluded that chain convergence was good.

To test how the limb darkening coefficients affect the derived system parameters, we repeated the MCMC procedure also fitting for the linear LD “ a ” which is the most sensitive to the observing filter. The quadratic LD coefficient, $b = 0.210172$, was kept fixed, because as reported by Gibson et al. (2008), the high precision of the RISE light curves is not enough to fully constrain the LD coefficients (i.e., the MCMC does not converge when fitting both coefficients). We restricted the linear LD coefficient to be the same for all the light curves since they were all taken with the same filter. Therefore, in the second MCMC procedure we fitted 13 parameters. We estimated $a = 0.337 \pm 0.034$.

4 RESULTS

Comparing the fitted and fixed LD solutions, we concluded that although the fitted linear LD coefficient is statistically significantly different from the theoretical value, this does not affect the derived system parameters to any extent. The two solutions are within 1.5σ of each other. Contrary to what was found by other authors (e.g., Gibson et al. 2008; Southworth 2008), the uncertainties of the fitted LD solution are slightly smaller than those of the fixed solution. The χ^2 of the fitted LD solution is similar to the fixed LD solution which does not justify the addition of an extra free parameter in the fit. Consequently, we conclude that our light curve is of insufficient

Table 1. Time residuals from the linear ephemeris.

| Epoch | Time residuals (sec) | Uncertainty (sec) |
|-------|----------------------|-------------------|
| -78 | 11 | 40 |
| 0 | -7 | 24 |
| 102 | 8 | 30 |

Table 2. WASP-21 system parameters derived from the mcmc

| Parameter | Value |
|---|---------------------------------|
| Normalised separation a/R_* | $9.68^{+0.19}_{-0.30}$ |
| Planet/star radius ratio R_p/R_* | $0.10705^{+0.00082}_{-0.00086}$ |
| Orbital inclination I [degrees] | 87.34 ± 0.29 |
| Impact parameter b [R_*] | $0.458^{+0.043}_{-0.036}$ |
| Transit duration T_T [days] | $0.1430^{+0.0013}_{-0.0010}$ |
| Stellar density ρ_* [ρ_\odot] | $0.652^{+0.041}_{-0.060}$ |

quality to better constrain the linear LD relative to that achieved by theoretical models and we choose to present the fixed LD solution.

The estimated transit times, combined the original ephemeris (Bouchy et al. 2010) were used to update the linear ephemeris,

$$T_i(HJD) = T(0) + EP. \quad (3)$$

We found $P = 4.3225060 \pm 0.0000031$ and $T_0 = 2455084.51974 \pm 0.00020$ which was set to the mid transit time of the 2009 light curve. This ephemeris was used in the final MCMC procedures.

For future reference, the time residuals from the linear ephemeris are given in Table 1. We conclude that the time residuals of WASP-21b are consistent with a linear ephemeris.

The geometric system parameters of WASP-21 and the 1σ uncertainties derived from the MCMC analysis with fixed limb darkening coefficients are given in Table 2. These parameters are directly measured from the transit light curve and are only weakly dependent of stellar properties through the limb darkening coefficients. Note, all the derived parameters presented in Table 2 were calculated at each point of the chain. Therefore, the final derived values and errors were determined from their probability distribution as done for the fitted values. We obtain a significantly lower density than was previous reported in the discovery paper $\rho_* = 0.84 \pm 0.09\rho_\odot$.

4.1 Stellar mass and age

To obtain the stellar and planetary physical properties, the geometric parameters have to be scaled with the stellar mass. The new high quality transit light curves give a direct estimate of the stellar density. This allows a more accurate estimation of stellar mass than $\log g$ derived from spectral analysis (Sozzetti et al. 2007). Currently there are two main methods to derive the stellar mass from the stellar density. The first uses isochrones and mass tracks from stellar models (Sozzetti et al. 2007) and the second uses an empirical calibration derived from stellar eclipsing binaries (Torres et al. 2010; Enoch et al. 2010).

Bouchy et al. (2010) derived the stellar mass through the empirical calibration between T_{eff} , ρ_* and $[\text{Fe}/\text{H}]$ (Torres et al. 2010) with the parametrisation of Enoch et al. (2010). Following the same procedure, with the improved ρ_* , we derive a stellar mass of

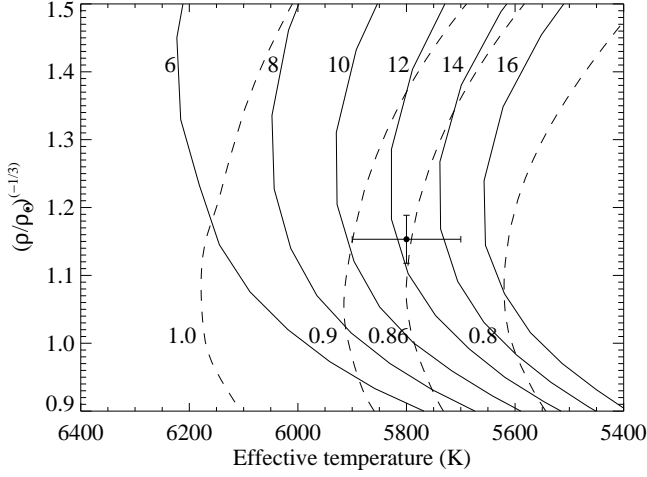


Figure 3. Isochrone models (solid lines) from Demarque et al. (2004) for WASP-21 using $[\text{Fe}/\text{H}] = -0.47$ and $[\text{M}/\text{H}] = -0.4$ from Bouchy et al. (2010). The age in Gyr is marked in the left of the respective model. We also show the mass tracks (dashed lines) for a stellar mass of 1.0, 0.9, 0.86 and $0.8 M_{\odot}$. We overplot the $T_{\text{eff}} = 5800$ value adapted from Bouchy et al. (2010) and the new $(\rho_*/\rho_{\odot})^{-1/3}$.

$1.02 \pm 0.05 M_{\odot}$. In Table 3 we present the mass and radius of WASP-21 and WASP-21b and the 1σ uncertainties derived from the MCMC for a stellar mass of $1.02 \pm 0.05 M_{\odot}$. We obtain a significantly larger stellar and planetary radius than previously reported. This is due to the main-sequence assumption in the previous analysis which as discussed below is found to be invalid.

We also estimate the stellar mass from stellar models by interpolating the Yonsei-Yale stellar evolution tracks by Demarque et al. (2004) using the metallicity from Bouchy et al. (2010). These evolution tracks are plotted in Figure 3 along with the position of WASP-21. From the isochrones, we estimate a lower mass of $0.86 \pm 0.04 M_{\odot}$ and an age of 12 ± 2 Gyr for WASP-21. In Figure 4, we also show the evolutionary tracks for stellar masses of 1.0, 0.95, 0.86 and $0.8 M_{\odot}$ adapted from Demarque et al. (2004). These suggest that WASP-21 is close to, or is already in the hydrogen-shell burning phase and hence is evolving off the main-sequence. This implies that the assumption of a main sequence mass-radius relationship in the original analysis of Bouchy et al. (2010) is faulty.

There is a significant difference between the mass derived from evolutionary models, $M_* = 0.86 \pm 0.04 M_{\odot}$, and the mass derived from the empirical calibration, $M_* = 1.02 \pm 0.05 M_{\odot}$. In the past, the Torres et al. (2010) calibration was found to be in agreement and a more straight-forward alternative to the stellar models (Torres et al. 2010; Enoch et al. 2010). Moreover, it has the advantage that it can be directly included in a transit fitting procedure (Enoch et al. 2010). However, recently the same discrepancy between empirical and isochrone masses was also found for WASP-37 (Simpson et al. 2011) and WASP-39 (Faedi et al. 2011). The Torres et al. (2010) eclipsing binaries sample used for calibrating their relationship does not contain many low-metallicity systems, in particular in the low-mass regime. Therefore, this suggests that the Torres et al. (2010) calibration might not hold for metal poor stars specially in the low mass regime. For these reasons, for WASP-21, we favour the lower mass derived from the evolution models. For a stellar mass of $M_* = 0.86 \pm 0.04 M_{\odot}$ we present the stellar and planetary radii for the WASP-21 system in Table 3 along with the 1σ uncertainties derived from the MCMC analysis.

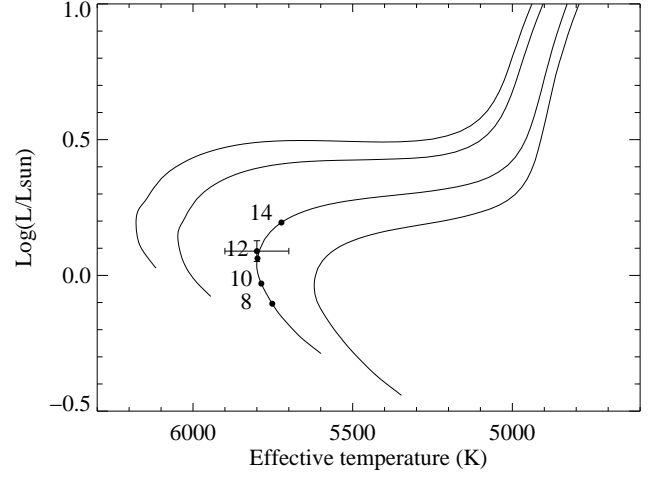


Figure 4. Evolutionary mass tracks from Demarque et al. (2004) for the same stellar parameters as Fig. 3 from left to right for stellar masses of 1.0, 0.95, 0.86 and $0.8 M_{\odot}$. WASP-21 position is in the $0.86 M_{\odot}$ evolutionary mass track for which we also show the 8, 10, 12, and 14 Gyr points.

Table 3. WASP-21 system stellar and planetary parameters derived using either the empirical calibration of Torres et al. (2010) or the YY stellar models (Demarque et al. 2004).

| | Torres models | YY models |
|--|---------------------------|---------------------------|
| Stellar mass M_* [M_{\odot}] | 1.02 ± 0.05 | 0.86 ± 0.04 |
| Stellar radius R_* [R_{\odot}] | $1.161^{+0.037}_{-0.024}$ | $1.097^{+0.035}_{-0.022}$ |
| Stellar surface gravity $\log g_*$ [cgs] | 4.32 ± 0.02 | 4.29 ± 0.02 |
| Orbital semimajor axis a [AU] | 0.052 ± 0.001 | 0.0494 ± 0.0009 |
| Planet mass M_p [M_{Jup}] | 0.30 ± 0.01 | 0.27 ± 0.01 |
| Planet radius R_p [R_{Jup}] | $1.210^{+0.048}_{-0.032}$ | $1.143^{+0.045}_{-0.030}$ |
| Planet density ρ_p [ρ_J] | $0.171^{+0.014}_{-0.018}$ | $0.181^{+0.015}_{-0.020}$ |
| Planet surface gravity $\log g_p$ [cgs] | 2.71 ± 0.02 | 2.71 ± 0.02 |

To summarise, we derive a lower stellar mass, $0.86 \pm 0.04 M_{\odot}$, and a lower planetary mass, $0.27 \pm 0.01 M_{\text{Jup}}$. We estimate the inclination of the orbit to be 87.3 ± 0.3 degrees. The radius of the star is found to be $1.10 \pm 0.03 R_{\odot}$ and the planet radius is $1.14 \pm 0.04 R_{\text{Jup}}$, yielding a planetary density of $0.18 \pm 0.02 \rho_J$.

4.2 Eccentricity

Bouchy et al. (2010) found the eccentricity to be statistically indistinguishable from zero, i.e. the χ^2 does not significantly improve when adding the two additional parameters to the circular model. For these cases, allowing the eccentricity to float tends to overestimate the eccentricity (Lucy & Sweeney 1971). Hence, Bouchy et al. (2010) adopted a circular orbit. Assuming a tidal dissipation parameter between 10^5 and 10^6 , the circularisation timescale for WASP-21b is approximately between 0.017 and 0.17 Gyr, respectively. Since this is much shorter than the derived age for the system we expect a circular orbit. However, if the orbit not circular assuming a zero eccentricity results in underestimated uncertainties. Therefore, it is interesting to investigate the effect of a small non-zero eccentricity in the system parameters and their uncertainties. As an example, we assume an eccentricity of 0.04 ± 0.04 which is consistent with the discovery paper. We

repeated the MCMC procedure allowing the eccentricity to float. Because the transit light curves do not constrain the eccentricity, we include a prior on the eccentricity of the form:

$$\frac{(ecc - ecc_0)^2}{\sigma_{ecc}^2}, \quad (4)$$

where we assume $ecc_0 = \sigma_{ecc} = 0.04$. This prior is added to equation 1 at each step of the chain. From the posterior eccentricity distribution we obtain an eccentricity of 0.038 ± 0.036 which is close to the input value.

The maximum effect of the eccentricity upon the derived parameters corresponds to the case where the transit occurs close to periastron ($\omega = 90^\circ$) or apastron ($\omega = -90^\circ$). Hence, in order to investigate the maximum deviation from a circular orbit we assume $\omega = 90^\circ$. For this particular case by assuming a circular orbit we would be overestimating a/R_* , inc and ρ_* , and underestimating the stellar and planetary masses and radii. The opposite would have happened if we have assumed $\omega = -90^\circ$.

The derived eccentric solution is within one sigma of the circular solution and the uncertainties of a/R_* , I and ρ_* are $\sim 30\%$ larger. This results in an increased uncertainty of $\sim 30\%$ on the radii and $\sim 20\%$ on the masses. Hence, we conclude that if the orbit eccentricity is < 0.038 the system parameters would be within $\sim 1.3\sigma$ of the values given in Tables 2 and 3.

5 DISCUSSION AND CONCLUSION

We have presented two high quality transit light curves of WASP-21b taken with RISE. Together with the previous RISE partial transit, these were fitted with an MCMC procedure to update the parameters of the system. We have been conservative in our error estimates by scaling the χ^2 and by including time correlated noise in our analysis.

The derived stellar density $\rho_* = 0.65 \pm 0.05\rho_\odot$ and the estimated age for the system, 12 ± 2 Gyr, suggest that WASP-21 is in the process of evolving off the main sequence. Therefore, the main-sequence mass-radius relation assumed for WASP-21 in the discovery paper was invalid which led to a significant overestimation of the stellar density, thus affecting the derived planetary properties. Using the stellar models of Demarque et al. (2004), we derived a significantly lower stellar, $M_* = 0.86 \pm 0.03M_\odot$, and planetary mass, $M_p = 0.27 \pm 0.01M_{Jup}$. This lower host star mass somewhat compensates the lower stellar density which results in a stellar radius which is within 1σ of the one presented by Bouchy et al. (2010).

We obtained a slightly larger planetary radius, $R_p = 1.14 \pm 0.04 R_{Jup}$, for WASP-21b than previously reported. Fortney et al. (2007) hydrogen/helium coreless models predict a radius of $\sim 1.06 R_\odot$ which is consistent within 2σ with our estimated radius without the need for any extra heating mechanism. Following Laughlin et al. (2011) we compute a radius anomaly, $\mathcal{R} = 0.09$, for WASP-21b. This supports the correlation reported by Laughlin et al. (2011), i.e. $\mathcal{R} = T_{equ}^{1.4}$, where T_{equ} is the equilibrium temperature of the planet, which is ~ 1320 K for WASP-21b. Bouchy et al. (2010) argued that the density of WASP-21b strengthens the correlation between planetary density and host star metallicity for hot Saturns (Guillot et al. 2006). With the addition of the latest Saturn-mass planet discoveries (e.g. WASP-39, Faedi et al. 2011; WASP-40, Anderson et al. 2011) this correlation appears weaker. However, if we scale for the equilibrium temperature with, for example \mathcal{R} , the correlation with metallicity is still

strong (see Figure 6 in Faedi et al. 2011). Moreover, the correlation also holds for the more massive planets (see Figure 3 in Laughlin et al. 2011).

Exoplanet transit light curves are often affected by systematic noise that can in some cases dominate the photometric noise. Therefore, it is important to minimise the sources of systematic noise. In Section 3.1, we show an example of systematic noise present in our exoplanet transit observations and suggest that the first step to decrease this noise is to maintain the star in the same pixel position in the CCD during the observations. We confirm that defocused observations can also help decreasing systematic noise, as well decreasing deadtime losses and hence improving the signal-to-noise (Southworth et al. 2009). The systematic noise in our observations was due to the variation of the stellar position across the CCD.

6 ACKNOWLEDGEMENTS

FPK is grateful to AWE Aldermaston for the award of a William Penny Fellowship. The RISE instrument mounted at the Liverpool Telescope was designed and built with resources made available from Queen's University Belfast, Liverpool John Moores University and the University of Manchester. The Liverpool Telescope is operated on the island of La Palma by Liverpool John Moores University in the Spanish Observatorio del Roque de los Muchachos of the Instituto de Astrofísica de Canarias with financial support from the UK Science and Technology Facilities Council. We thank Tom Marsh for the use of the ULTRACAM pipeline. SCCB is grateful to Catherine Walsh for proofreading this paper and to Yilen Gmez Maqueo Chew for useful comments.

REFERENCES

- Anderson D. R., Barros S. C. C., Boisse I., Bouchy F., Collier-Cameron A., Faedi F., Hebrard G., Hellier C., Lendl M., Moutou C., Pollacco D., Santerne A., Smalley B., Smith A. M. S., Todd I., et al. 2011, ArXiv e-prints
- Bouchy F., Hebb L., Skillen I., Collier Cameron A., Smalley B., Udry S., Anderson D. R., Boisse I., Enoch B., Haswell C. A., Hébrard G., Hellier C., Joshi Y., Kane S. R., Maxted P. F., Mayor M., Moutou C., Pepe F., et al. 2010, A&A, 519, A98+
- Carter J. A., Winn J. N., 2009, ApJ, 704, 51
- Collier Cameron A., Wilson D. M., West R. G., Hebb L., Wang X., Aigrain S., Bouchy F., Christian D. J., Clarkson W. I., Enoch B., Esposito M., Guenther E., Haswell C. A., Hébrard G., et al. 2007, MNRAS, 380, 1230
- Demarque P., Woo J., Kim Y., Yi S. K., 2004, ApJS, 155, 667
- Dhillon V. S., Marsh T. R., Stevenson M. J., Atkinson D. C., Kerry P., Peacocke P. T., Vick A. J. A., Beard S. M., Ives D. J., Lunney D. W., McLay S. A., Tierney C. J., Kelly J., Littlefair S. P., Nicholson R., Pashley R., Harlaftis E. T., O'Brien K., 2007, MNRAS, 378, 825
- Enoch B., Collier Cameron A., Parley N. R., Hebb L., 2010, A&A, 516, A33+
- Faedi F., Barros S. C. C., Anderson D. R., Brown D. J. A., Collier Cameron A., Pollacco D., Boisse I., Hebrard G., Lendl M., Lister T. A., Smalley B., Street R. A., Triaud A. H. M. J., et al. 2011, ArXiv e-prints
- Fortney J. J., Marley M. S., Barnes J. W., 2007, ApJ, 659, 1661
- Gelman A., Rubin D., 1992, Statistical Science, 7, 457

- Gibson N. P., Pollacco D., Simpson E. K., Joshi Y. C., Todd I., Benn C., Christian D., Hrudková M., Keenan F. P., Meaburn J., Skillen I., Steele I. A., 2008, *A&A*, 492, 603
- Gillon M., Smalley B., Hebb L., Anderson D. R., Triaud A. H. M. J., Hellier C., Maxted P. F. L., Queloz D., Wilson D. M., 2009, *A&A*, 496, 259
- Guillot T., 2005, *Annual Review of Earth and Planetary Sciences*, 33, 493
- Guillot T., Santos N. C., Pont F., Iro N., Melo C., Ribas I., 2006, *A&A*, 453, L21
- Howarth I. D., 2011, *MNRAS*, 413, 1515
- Joshi Y. C., Pollacco D., Cameron A. C., Skillen I., Simpson E., Steele I., Street R. A., Stempels H. C., Christian D. J., Hebb L., Bouchy F., Gibson N. P., Hébrard G., Keenan F. P., Loeillet B., et al. 2009, *MNRAS*, 392, 1532
- Laughlin G., Crismani M., Adams F. C., 2011, *ApJL*, 729, L7+
- Lucy L. B., Sweeney M. A., 1971, *AJ*, 76, 544
- Mandel K., Agol E., 2002, *ApJL*, 580, L171
- Pollacco D. L., Skillen I., Cameron A. C., Christian D. J., Hellier C., Irwin J., Lister T. A., Street R. A., West R. G., Anderson D., Clarkson W. I., Deeg H., Enoch B., Evans A., Fitzsimmons A., Haswell C. A., Hodgkin S., et al. 2006, *PASP*, 118, 1407
- Simpson E. K., Faedi F., Barros S. C. C., Brown D. J. A., Collier Cameron A., Hebb L., Pollacco D., Smalley B., Todd I., Butters O. W., Hébrard G., McCormac J., Miller G. R. M., Santerne A., Street R. A., Skillen I., Triaud A. H. M. J., et al. 2011, *AJ*, 141, 8
- Southworth J., 2008, *MNRAS*, 386, 1644
- Southworth J., Hinse T. C., Jørgensen U. G., Dominik M., Ricci D., Burgdorf M. J., Hornstrup A., Wheatley P. J., Anguita T., Bozza V., et al. 2009, *MNRAS*, 396, 1023
- Sozzetti A., Torres G., Charbonneau D., Latham D. W., Holman M. J., Winn J. N., Laird J. B., O'Donovan F. T., 2007, *ApJ*, 664, 1190
- Steele I. A., Bates S. D., Gibson N., Keenan F., Meaburn J., Mottram C. J., Pollacco D., Todd I., 2008, in *Society of Photo-Optical Instrumentation Engineers (SPIE) Conference Series* Vol. 7014 of *Society of Photo-Optical Instrumentation Engineers (SPIE) Conference Series*, RISE: a fast-readout imager for exoplanet transit timing
- Tegmark M., Strauss M. A., Blanton M. R., Abazajian K., Dodelson S., Sandvik H., Wang X., Weinberg D. H., Zehavi I., Bahcall N. A., Hoyle F., Schlegel D., Scoccimarro R., Vogeley M. S., et al. 2004, *PhRvD*, 69, 103501
- Torres G., Andersen J., Giménez A., 2010, *A&ARV*, 18, 67